

Photolysis of Hi-CO Nitrogenase – Observation of a Plethora of Distinct CO Species Using Infrared Spectroscopy

Lifen Yan,^[a] Christie H. Dapper,^[b] Simon J. George,^[a,c] Hongxin Wang,^[a,c]
Devrani Mitra,^[a] Weibing Dong,^[a] William E. Newton,^[b] and Stephen P. Cramer*^[a,c]

Keywords: Nitrogen fixation / Nitrogenases / Enzyme catalysis / Carbon monoxide / IR spectroscopy / Photolysis / *Azotobacter vinelandii*

Fourier-transform infrared-spectroscopy (FT-IR) was used to study the photochemistry of CO-inhibited *Azotobacter vinelandii* Mo nitrogenase using visible light at cryogenic temperatures. The FT-IR difference spectrum of photolyzed hi-CO at 4 K comprises negative bands at 1973 cm⁻¹ and 1679 cm⁻¹ together with positive bands at 1711 cm⁻¹, 2135 and 2123 cm⁻¹. The negative bands are assigned to a hi-CO state that comprises 2 metal-bound CO ligands, one terminally bound, and one bridged and/or protonated species. The positive band at 1711 cm⁻¹ is assigned to a lo-CO product with a single bridged and/or protonated metal-CO group. We term these species “Hi-1” and “Lo-1”, respectively. The high-energy bands are assigned to a liberated CO trapped in the protein pocket. Warming results in CO recombination, and the temperature dependence of the recombination rate yields an activation energy of 4 kJ mol⁻¹. Two α -H195 variant

enzymes yielded additional signals. Asparagine substitution, α -H195N, gives a spectrum containing 2 negative “Hi-2” bands at 1936 and 1858 cm⁻¹ with a positive “Lo-2” band at 1780 cm⁻¹, while glutamine substitution, α -H195Q, produces a complex spectrum that includes a third CO species, with negative “Hi-3” bands at 1938 and 1911 cm⁻¹ and a positive feature “Lo-3” band at 1921 cm⁻¹. These species can be assigned to a combination of terminal, bridged, and possibly protonated CO groups bound to the FeMo cofactor active site. The proposed structures are discussed in terms of both CO inhibition and the mechanism nitrogenase catalysis. Given the intractability of observing nitrogenase intermediates by crystallographic methods, IR-monitored photolysis appears to be a promising and information-rich probe of nitrogenase structure and chemistry.

Introduction

The mechanism by which the enzymatic nitrogen fixation system known as nitrogenase (N₂ase) catalyzes the reduction of dinitrogen to ammonia at moderate temperatures and pressures remains only partially understood.^[1] For the Mo-dependent N₂ase, binding of all known substrates and inhibitors involves the MoFe₇S₉X-homocitrate-containing prosthetic group, usually called the FeMo cofactor, of the larger MoFe-protein. ENDOR (electron nuclear double resonance) spectroscopy of native and variant N₂ases has helped define the interaction of bound intermediates with the FeMo cofactor at various states of reduction.^[2] However, additional complementary techniques

are still needed to characterize N₂ase interactions with substrates and inhibitors, preferably over a variety of time scales and temperatures.

As a powerful inhibitor, CO is a valuable probe of the ligand binding properties of the FeMo cofactor active site, and a proper understanding of this chemistry should give substantial insights into the mechanism of N₂ase. CO interactions with N₂ase have taken on added significance with the report of hydrocarbon synthesis (Fischer–Tropsch chemistry) during CO reactions with vanadium N₂ase.^[3] Although this discovery of CO reactivity is new, the inhibition of nitrogen fixation by CO has been known since at least 1941.^[4] CO inhibits the reduction of N₂ and other substrates reversibly and non-competitively,^[5] at micromolar concentrations and on a sub-second time scale consistent with the rate of electron transfer.^[6] CO does not, however, inhibit H₂ evolution by N₂ase so that, under CO, N₂ase effectively becomes an ATP-dependent H₂ase.

The CO binding chemistry of N₂ase is complex with several CO-bound states, some involving more than one bound CO and more than one binding site, and with some different CO-bound states known to readily interconvert.^[6] CO binding is also sensitive to amino acid substitutions in the protein pocket.^[6d] Hence CO can be used to investigate

[a] Department of Applied Science, University of California, One Shields Avenue, Davis, CA 95616, USA
Fax: +1-530-752-2444
E-mail: spjcramer@ucdavis.edu

[b] Department of Biochemistry, Virginia Polytechnic Institute and State University, 123 Engel Hall, Blacksburg, VA 24061, USA

[c] Physical Biosciences Division, Lawrence Berkeley National Laboratory, 1 Cyclotron Road, MS 6R2100, Berkeley, CA 94720, USA

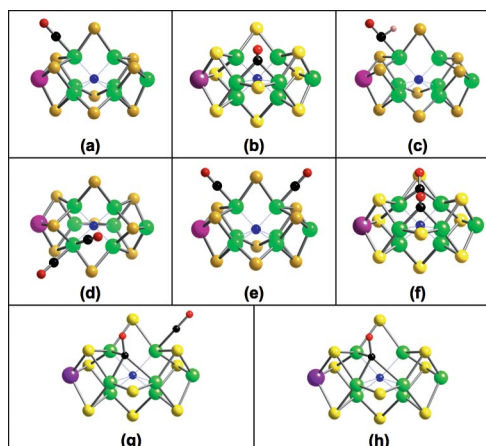
Supporting information for this article is available on the WWW under <http://dx.doi.org/10.1002/ejic.201100029>.

both FeMo cofactor small molecule binding sites, as well as the interactions of bound ligands with neighbouring amino acids. In this work, we have used FT-IR (Fourier-transform infrared) spectroscopy to monitor the low temperature photolysis of CO-inhibited *Azotobacter vinelandii* N₂ase and selected variant enzymes in order to identify the vibrational frequencies associated with bound and free CO. The results are compared with related photolysis studies monitored by EPR^[7] as well as with previous stopped-flow FT-IR studies (SF-FT-IR).^[6]

Exposure of N₂ase to CO during turnover elicits species with a variety of EPR signals, depending on the partial pressure of CO (*p*CO).^[8] However, these EPR signals develop over a longer time scale than required for substrate inhibition.^[6c] Each of these species and its characteristic EPR signal is described by the *p*CO required for its formation. Thus, the species and its axial *S* = 1/2 EPR signal (*g* values near 2.17 and 2.06) are both called “hi-CO” and are formed under a *p*CO many times higher than required for substrate inhibition. This hi-CO N₂ase species is reported to contain two CO molecules bound to the FeMo cofactor. A species with an *S* = 1/2 rhombic EPR spectrum (*g* values of 2.09, 1.98, and 1.93) is called “lo-CO” because it forms under a much lower *p*CO that is comparable to that required for inhibition and contains only one bound CO. A third species and EPR signal with apparent *g* values about 5.78, 3.7, and 2.7, both called hi(5)-CO, have also been identified under high *p*CO. Mainly based on ENDOR spectroscopic studies, the lo-CO EPR signal has been described as arising from a FeMo cofactor cluster with a single bridging CO, the hi(5)-CO signal from a cluster with two bridging CO ligands, and the hi-CO signal from a cluster with one terminal CO ligand on each of two adjacent Fe atoms. A sampling of the Fe-centred CO-binding modes that have been proposed is illustrated in Scheme 1.

The appearance of the CO-induced EPR signals changes when the native amino acids around the FeMo cofactor active site are substituted by other residues, and not all of these signals are generated when such variant N₂ases are turned over under CO.^[8h] In past studies, only four of ten Av1 variants (wild-type, $\Delta nifV$, α -H195Q, and α -R96Q) generated the hi-CO signal, whereas only one (α -R277H) failed to generate the lo-CO signal, and only one (α -Q191K) failed to generate the hi(5)-CO signal. Despite complete inhibition of N₂-reduction activity, the EPR signal integrations often account for less than a third of the FeMo cofactor present in the samples.^[8g] Furthermore, the VFe protein in V-N₂ase generated none of these CO-induced EPR signals during turnover, even though CO still acts as a reversible inhibitor of V-N₂ase-catalyzed substrate reduction,^[8b] and despite the more recent discovery of hydrocarbon synthesis in the presence of CO.^[3] Obviously, EPR-silent forms with bound CO must either co-exist with and/or replace the known EPR-active hi-CO, lo-CO, and hi(5)-CO species.

Complementing the EPR data are results from SF-FT-IR experiments over the range 2200–1700 cm⁻¹.^[6] In these experiments, hi-CO and lo-CO were defined in terms of the



Scheme 1. Proposed Fe-based modes of CO binding in N₂ase: (a) single terminal a-top CO,^[6b] (b) single bridging CO,^[8e] (c) “formyl” CO, (d) two terminal a-top CO, same Fe,^[6b] (e) two terminal a-top CO, different Fe,^[8e] (f) two bridging CO,^[8h] (g) triple-bridging and terminal CO, (h) triple-bridging CO. Mo histidine and homocitrate ligands and cysteine thiolate ligand of Fe-1 have been omitted for clarity. No attempt was made to relax the Fe-S framework for these structures. Atom color codes: Fe green, Mo purple, S yellow, C black, O red. The undefined central atom of FeMo-co is printed in blue.

ratio of CO concentration [CO] to Mo content in the enzyme [Mo]. With less than stoichiometric [CO]/[Mo] (lo-CO), a single CO band appeared at 1904 cm⁻¹ and peaked in intensity rapidly (within ca. 7 s) before decaying. With excess [CO] (hi-CO), a pair of new CO bands at 1936 cm⁻¹ and 1880 cm⁻¹ were observed to form with the same rate while an independent band at 1958 cm⁻¹ was also observed. All of these species were assigned to terminally bound CO molecules. After relatively long times (> 10 s), under low [CO] the 1904 cm⁻¹ peak decayed while a new CO band at 1715 cm⁻¹ developed. To explain the low energy of this band, CO doubly or triply bridging to a face of the FeMo cofactor was suggested (Scheme 1, b and h), and the possibility of Fe-formyl complexes was also considered (Scheme 1, c). Other CO-related IR bands have been observed during spectroelectrochemical studies of isolated FeMo-co,^[9] where features at 1808 and 1835 cm⁻¹ were proposed to arise from bridging CO, whereas bands at 1885 and 1920 cm⁻¹ were assigned to terminally bound CO species. Each of these bands is presumed to represent a different CO-bound FeMo-co species in a different cluster redox level, protonation state and/or CO-binding geometry.

Despite the wealth of data, considerable debate surrounds the proposed structures. For example, some theoretical calculations indicate that steric repulsions between CO and adjacent sulfides would destabilize doubly bridged structures.^[10] Plane-wave DFT calculations also failed to find a stable bridging CO structure for a variety of models.^[11] Using an 8-Fe model for the FeMo cofactor, the most stable CO structure was found to involve terminal CO in an “*exo*” geometry (Scheme 1, a) at the 3-electron, 3-proton reduction level.^[12] The alternative of terminal CO binding at Mo has also been proposed to explain some of the spec-

troelectrochemical FT-IR results from studies of isolated FeMo-co.^[9]

Given the ambiguity surrounding the proposed structures for CO-bound N₂ase, we decided to investigate these CO-bound species using photolysis under cryogenic conditions with FT-IR detection of the spectral changes. The photosensitivity of metal carbonyl complexes is well-known, and in bioinorganic chemistry, photolysis has been employed to study CO binding to heme proteins^[13] and to hydrogenases.^[14] Maskos and Hales discovered the light sensitivity of the hi-CO form of N₂ase, and using EPR spectroscopy, they demonstrated conversion of the hi-CO to the lo-CO species at low temperatures, and subsequent recombination to the hi-CO species at higher temperatures with an activation energy of ca. 4 kJ mol⁻¹.^[7] In addition to wild-type N₂ase, we studied two variant proteins: α -H195Q and α -H195N. These are of particular interest as they bind, but do not reduce N₂ well or at all, respectively and it has been suggested that the α -H195 residue plays a role in channeling protons to the FeMo cofactor active site.^[15]

Results

Our experimental strategy was to prepare concentrated (ca. 500 μ M Mo) samples of hi-CO N₂ase under conditions known to give high yields of the *S* = 1/2 hi-CO EPR signal. Samples were frozen and for each sample a baseline IR spectrum was collected. Photolysis was then performed using visible light over 30–300 minutes at a temperature of 4 K. Periodically, the photolysis was stopped and an IR spectrum was collected. We present our data as a series of light-induced IR difference spectra depending on the time of photolysis. The initial pre-photolysis spectrum is subtracted from each spectrum collected during photolysis, giving spectra with negative bands from the starting materials while products produce positive features. In order to identify CO-dependent features we prepared parallel samples using ¹³CO and ¹³C¹⁸O isotopomers. We also monitored the recombination kinetics as a function of temperature. Although our initial experiments employed an H₂O based buffer, most of our results used D₂O buffers as this allows measurements to be extended to 1750–1550 cm⁻¹.

The Dominant IR-Detected CO-Related Photolysis Features

Figure 1 shows the time course of changes at the higher-frequency edge of a water window in the IR spectra for hi-CO N₂ase samples illuminated with visible light at ca. 4 K in an H₂O-based buffer, as well as spectra over a wider range in a D₂O-based buffer. In these spectra, the natural abundance hi-CO samples exhibit a sharp negative band at ca. 1973 cm⁻¹, which shifts to 1928 or 1881 cm⁻¹, respectively when hi-¹³CO or hi-¹³C¹⁸O samples are photolyzed. By analogy with previous EPR-monitored photolysis studies, these changes presumably reflect the photolytic loss of a bound CO molecule from hi-CO N₂ase, creating a lo-CO species together with a “free CO”.^[7] There was no indica-

tion of a negative difference band at 1936 cm⁻¹, which might have correlated with the dominant IR band observed by SF-FT-IR.^[6]

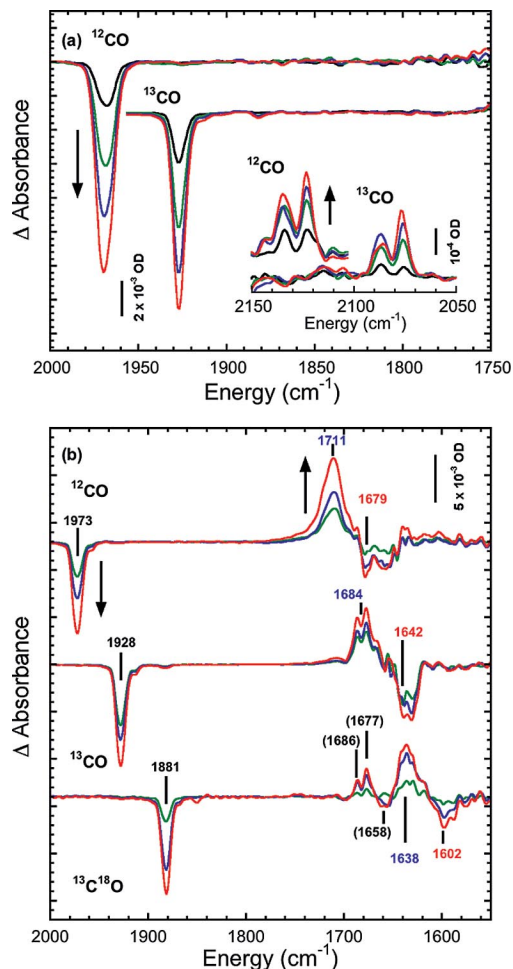


Figure 1. Time-dependent absorbance changes upon photolysis of hi-CO N₂ase showing the Hi-1 pattern of signals. (a) Using aqueous buffer and (top) ¹²CO or (bottom) ¹³CO. Inset: development of features in 2050–2150 cm⁻¹ region. (b) Extension to the lower energy region using D₂O buffer: ¹²CO (top), ¹³CO (middle), and ¹³C¹⁸O (bottom). Bands in parentheses are assigned to the protein or homocitrate modes. Photolysis times and conditions for each spectrum are in the Supporting Information.

Production of “free CO” during photolysis is confirmed by examination of the higher energy region, where photolysis causes the appearance of two bands split by 12 cm⁻¹ at 2135 and 2123 cm⁻¹, shifting to 2087 and 2076 cm⁻¹ when ¹³CO is used (see part a of Figure 1, inset). These bands reflect CO trapped relatively near the FeMo cofactor. For comparison, after low-temperature photolysis of myoglobin-bound CO (Mb-CO), a fraction of the CO is trapped in the Mb “docking site” in either of two orientations, also split by 12 cm⁻¹ at 2131 and 2119 cm⁻¹.^[13] It thus appears that in N₂ase, CO can also be trapped in two orientations within a protein pocket.

Initially, we expected to see a positive band at 1904 cm⁻¹ to reflect formation of a lo-CO species, because this is where the first CO band emerges in SF-FT-IR experiments

under lo-CO conditions.^[6a–6c] However, there is no photolysis feature near 1904 cm^{-1} , and instead the largest positive absorbance change for “hi- ^{12}CO ” is at 1711 (1684, 1638) cm^{-1} (Figure 1, b). (Here and in the remainder of this paper, numbers following in parentheses refer to spectra for experiments with ^{13}CO and, when available, $^{13}\text{C}^{18}\text{O}$ isotopomers, respectively.) This 1711 cm^{-1} band presumably corresponds to the more slowly-appearing, long-lived (> 10 min) band at 1715 cm^{-1} seen in the SF-FT-IR experiments.^[6]

If the original hi-CO species indeed involved a structure with two terminally bound CO molecules, then two negative bands might be expected in the photolysis difference spectrum. This is because even if only one of the two CO molecules were photolyzable under the current conditions, the frequency of the remaining CO would be expected to change when the other CO is photolyzed. However, above 1700 cm^{-1} only one negative band at 1973 cm^{-1} is visible. It therefore seems that the two CO molecules bound in the hi-CO sample must either have very similar (within ca. 4 cm^{-1}) stretching frequencies or have very different frequencies, with the second CO band below 1700 cm^{-1} .

In fact, the lower frequency region of the ^{12}CO photolysis spectrum (Figure 1, b) shows a negative feature at 1679 cm^{-1} . The appearance of this feature is complicated by the fact that this region also contains so-called “amide-I” features, as well as potential contributions from glutamine or asparagine side chains.^[16] However, with $^{13}\text{C}^{18}\text{O}$, we see that there are no negative protein or homocitrate bands in the 1680 cm^{-1} region, only a pair of weak positive bands at 1686 and 1677 cm^{-1} and a dip at 1658 cm^{-1} . Conclusive identification of the 1679 cm^{-1} feature as a CO-related species thus comes from comparing the photolysis difference spectra for the three different CO isotopomer samples, when the negative CO 1679 cm^{-1} band shifts by either about 37 or 77 cm^{-1} to 1642 or 1602 cm^{-1} , in line with predicted shifts of 37 and 78 cm^{-1} . With the perspective gained from data for all three isotopomers, the features superimposed on the CO bands can then be assigned as arising from the protein matrix. We refer to this first photolyzable species, with ^{12}CO bands at 1973 and 1679 cm^{-1} , as Hi-1, while the product species with a bound CO band at 1711 cm^{-1} is termed Lo-1. We label the free (“in the pocket”) CO species as B by analogy with MbCO nomenclature. Potential structural assignments are addressed in the discussion.

A Second CO-Related Photolysis Pair

We turn next to photolysis of CO-treated α -H195N Av1 (Figure 2). In both wild-type and α -H195Q Av1, the side chains at the α -195 position contribute NH \rightarrow S hydrogen bonds to sulfur atom S2B of the FeMo cofactor,^[8g] but in the α -H195N variant, the shorter asparagine side chain cannot create such a bond.^[17] As shown in Figure 2, with α -H195N, the Hi-1 signals are no longer observable. Instead, a strong negative band at 1936 (1892) cm^{-1} and a weaker negative band at 1858 (1816) cm^{-1} are seen for the initial

state. A positive band at 1780 (1736) cm^{-1} , with a weaker positive band at 1760 (1717) cm^{-1} , can be associated with the photolysis product. With difficulty, bands associated with “free CO” photolysis could again be observed (Supporting Information). This additional photolyzable species will be referred to as Hi-2, and the resulting photoproduct will be referred to as Lo-2.

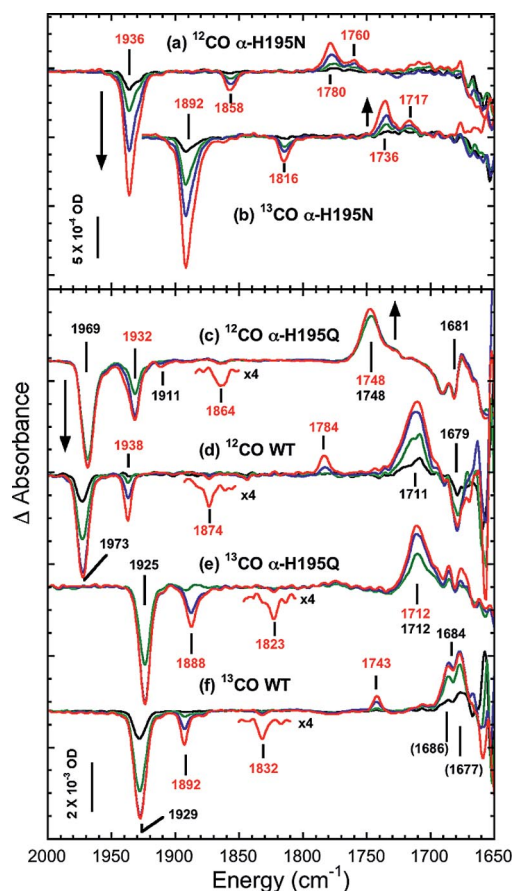


Figure 2. Evidence for the Hi-2 CO photolysis signal. Top panel: time-dependent absorbance changes upon second cycle of photolysis of hi-CO α -H195N Av1 using (a) ^{12}CO and (b) ^{13}CO in D_2O buffer. Data have been scaled to a common size for the higher frequency Hi-2 band. Bottom panel: time-dependent absorbance changes upon second cycle of photolysis of hi-CO “aged” wild-type (WT) and α -H195Q Av1 in D_2O buffer. (c) α -H195Q with ^{12}CO (d) wild-type with ^{12}CO (e) α -H195Q Av1 with ^{13}CO (f) wild-type with ^{13}CO . Red numbers refer to Hi-2 and Lo-2 features, black to Hi-1 and Lo-1 features, parentheses to protein or homocitrate modes. Photolysis times and conditions for each spectrum are in the Supporting Information.

We also examined the α -H195Q variant, which exhibits all three CO-based EPR signals.^[8g] With α -H195Q, not only is the Hi-1 species observed (in this case at 1969 cm^{-1}), but also a Hi-2 species, with a negative band at 1932 (1888, 1844) cm^{-1} (Figure 2, c and e). Inspection shows that development of the Hi-2 features occurs more slowly than those for Hi-1. As with α -H195N, there was also a second, weak negative band, in this case at 1864 (1823, 1779) cm^{-1} and a strong positive feature at 1748 (1712, 1677) cm^{-1} .

A Hi-2 species was also seen for wild type Av1, but only after storage of CO-inhibited enzyme in liquid nitrogen over a period of several months. As shown in parts d and f of Figure 2, in addition to the original Hi-1 and Lo-1 features, these stored wild-type samples showed a strong negative band at 1938 (1892) cm^{-1} , weaker negative features at 1874 (1832), and a positive band at 1784 (1743) cm^{-1} . Compared to the dip at 1938 cm^{-1} , the above-mentioned secondary negative bands associated with Hi-2 photolysis are relatively weak, and there often seem to be multiple species.

A Third Set of “Less Reversible” Photolysis Signals

In order to clearly present the features associated with Hi-2 and Lo-2 species, the spectra presented in Figure 2 are the photolysis spectra that were obtained during a second photolysis of the relevant hi-CO samples, after each had been subjected to a previous photolysis, followed by thermal cycling to 110 K and back to ca. 4 K. In Figure 3, the more complex patterns that are obtained during the first photolysis at 4 K are presented. With the α -H195Q variant, both the Hi-1 1969 cm^{-1} band and the Hi-2 band at 1932 cm^{-1} were observed. However, there is also a third signal, the strongest in the spectrum, with a negative band at a slightly higher frequency of 1938 cm^{-1} . This 6 cm^{-1} shift from Hi-2 was observed with each CO isotopomer (Figure 3). As shown in Figure 3, the 1938 cm^{-1} band appears at the same rate as a negative band at 1911 cm^{-1} and a positive feature at 1921 cm^{-1} , and these features as a group appear more slowly than the Hi-2 band at 1932 cm^{-1} . We refer to this new third species and its associated negative bands as

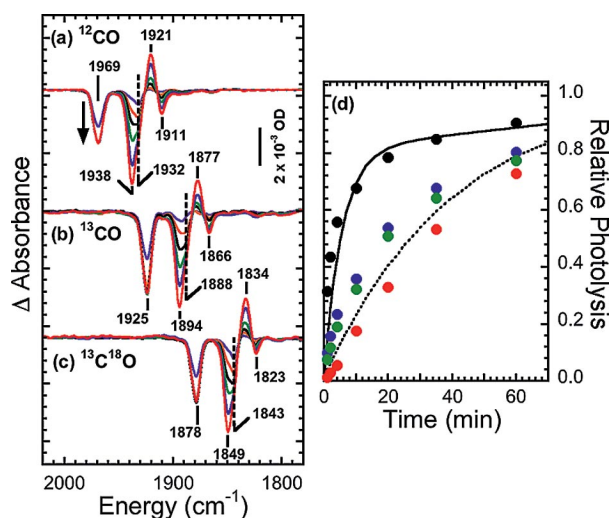


Figure 3. Evidence for “less reversible” photolysis signals revealed on the first photolysis cycle using hi-CO H195Q Av1 and (a) ^{12}CO , (b) ^{13}CO , or (c) $^{13}\text{C}^{18}\text{O}$. Photolysis times and conditions for each spectrum are in the Supporting Information. (d) The change in relative absolute intensities of Hi-3 and Lo-3 bands at 1938 (blue filled circle), 1911 (green filled circle), and 1921 (red filled circle) cm^{-1} , respectively, vs. the loss of the Hi-2 band at 1932 cm^{-1} (black filled circle). Smooth curves are least-squares fits only to guide the eye.

Hi-3, while the positive signal and associated product are labelled Lo-3. A weaker version of this signal is observed with the α -H195N variant.

Recombination Kinetics

The recombination dynamics for Lo-1 \rightarrow Hi-1 and Lo-2 \rightarrow Hi-2 reversions for wild-type and α -H195Q Av1, respectively, are presented in Figure 4. At 70 K, the Hi-1 negative band at 1973 (1928) cm^{-1} diminishes over minutes to hours. The “free CO” bands diminish at the similar rates (not shown), confirming that we are observing CO recombination. The early kinetic data for Hi-1 restoration can be modelled as an exponential decay with a single rate constant. At longer times, however, there is evidence for additional slower processes (Figure 4). An Arrhenius plot using the initial rate constants at various temperatures yields an activation energy of ca. 3.7 kJ mol^{-1} (Figure 4), in good agreement with the 3.9 kJ mol^{-1} value reported from EPR measurements.^[7]

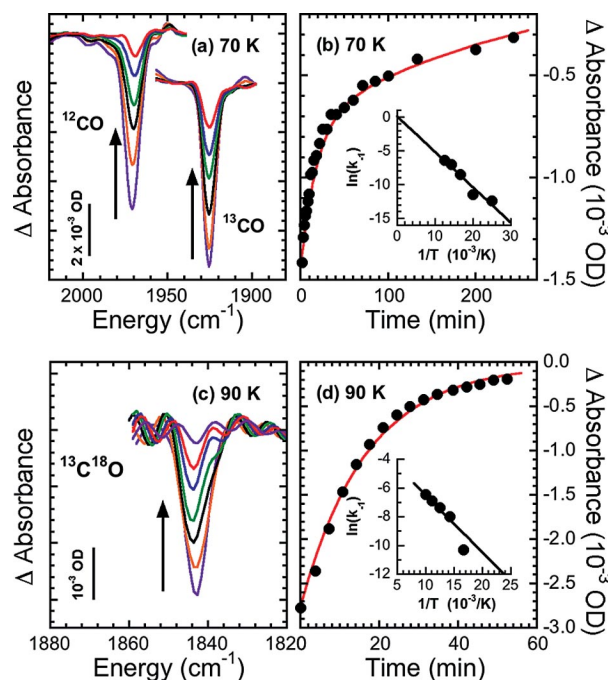


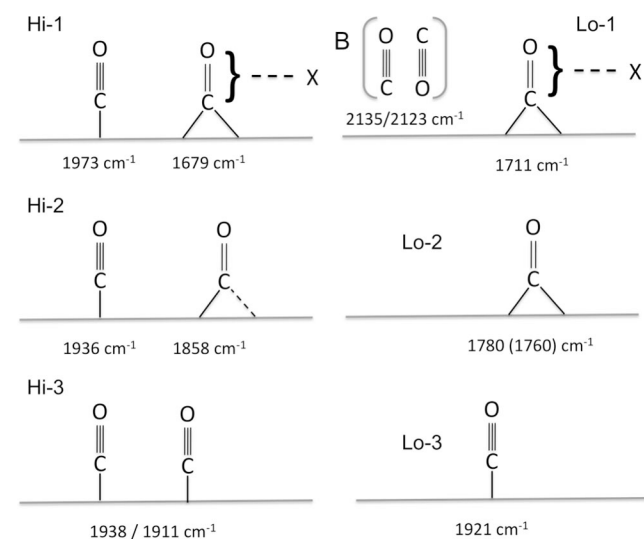
Figure 4. Recombination dynamics of wild-type Lo-1 to Hi-1 and α -H195Q Lo-2 to Hi-2. (a) Wild-type Lo-1 to Hi-1 spectra measured during recombination at 70 K of the ^{12}CO (top) and ^{13}CO (bottom). (b) typical dual exponential fit to time-dependent data. Inset: Arrhenius plot of $\ln(k_{-1})$ vs. $1/T$, using initial rate constants. (c) α -H195Q Lo-2 to Hi-2 spectra measured during recombination at 90 K using the $^{13}\text{C}^{18}\text{O}$ Hi-2 1843 cm^{-1} band. (d) typical single exponential fit to data for recombination of the 1843 cm^{-1} Hi-2 band. Inset: Arrhenius plot of $\ln(k_{-1})$ vs. $1/T$. Recombination times for each spectrum are in the Supporting Information.

Recombination of the Lo-2 \rightarrow Hi-2 species was also observed (Figure 4), and in the case of the α -H195Q Av1 $^{13}\text{C}^{18}\text{O}$ 1843 cm^{-1} band, a single exponential models the kinetics reasonably well over the first hour of this process. However, the fit is not perfect, and there is again evidence

for slower processes in the data. The activation energy derived from an Arrhenius plot was ca. 3.3 kJ mol^{-1} for α -H195Q. In contrast with Lo-1 \rightarrow Hi-1 and Lo-2 \rightarrow Hi-2 conversions, no evidence for recombination of Hi-3 to Lo-3 was seen up to 110 K. Clearly, additional studies over a wider range of temperatures will be of great interest.

Discussion

We have studied the photolysis of the hi-CO complexes of wild-type Av1 as well as the α -H195Q and α -H195N Av1 variant enzymes. We have observed 3 distinct sets of photolyzable hi-CO bands, each of which yields a different corresponding lo-CO species. For Hi-1 \rightarrow Lo-1 and Hi-2 \rightarrow Lo-2 photochemistry, we have also observed the formation of bands assigned to “free CO” – that is CO not coordinated to the FeMo cofactor but trapped in the protein pocket, and we can observe the recombination of this CO to form the original hi-CO species. In Table 1, we summarize the overall hi-CO photolysis results with the involved species



Scheme 2. Essential features of proposed pre- and post-photolysis species. X could be H and/or another metal. The dashed line indicates X could interact with C or O or both. The species labelled B refers to free CO in two different orientations in a protein pocket. The dashed line in the Hi-2 structure indicates possible semi-bridging interaction. Listed frequencies refer to bands for: wild-type (top), H195N (middle), H195Q (bottom).

characterized by their ^{12}CO frequencies. The complete data for all CO isotopes are presented in the Supporting Information. Scheme 2 summarizes our proposed structural assignments for the observed species.

Hi-1/Lo-1

What is the connection between our Hi-1 band at 1973 cm^{-1} and the bands previously observed at 1880, 1904, 1936 and 1960 cm^{-1} in SF-FT-IR studies^[6]? [We use the published SF-FT-IR values for Av1, although *Klebsiella pneumoniae* (Kp1) gave essentially the same results.] The closest correlate of our 1973 cm^{-1} band is the 1960 cm^{-1} feature that peaks over a period of ca. 10 seconds in the SF-FT-IR. The modest difference in frequency (13 cm^{-1}) between the 1973 and 1960 cm^{-1} photolysis and SF-FT-IR bands can be attributed to a slightly modified environment, possibly due to the use of cryogenic temperatures. It is not simply a solvent effect, because low temperature photolysis control experiments yielded the same frequency bands in the absence of ethylene glycol (see Supporting Information). For comparison, in Mb-CO, the dominant A_1 substate band at 1945 cm^{-1} is accompanied by an A_3 substate band at ca. 1930 cm^{-1} and an A_0 substrate band at 1966 cm^{-1} ; these features arise from essentially the same type of Fe–CO bonding, where different conformations have different electrostatic and H-bonding interactions with the imidazole side chain of the distal histidine.^[18] Environmental shifts over ca. 36 cm^{-1} are thus possible, and our 1973 cm^{-1} band and the SF-FT-IR 1960 cm^{-1} band are likely the same as far as the site and connectivity of CO bonding and the redox status of the FeMo cofactor are concerned. In any case, our 1973 cm^{-1} band almost certainly results from the photolytic loss of a terminally bound CO molecule (Scheme 2).

Our Lo-1 band at 1711 cm^{-1} is closest to the long-lived lo-CO band at 1715 cm^{-1} in the (Kp1) SF-FT-IR data.^[6b] This relatively low frequency has always been difficult to explain, and the problem is even greater for the second Hi-1 band at ca. 1679 cm^{-1} . For comparison, [FeFe] H_2 ases have H-cluster forms with doubly bridging CO molecules, but the bands for these species range from 1793 to 1848 cm^{-1} .^[14b,19] Bands as low as either 1790 or 1780 cm^{-1} are reported for bridging CO in $\text{Fe}^{\text{I}}\text{-Fe}^{\text{II}}$ and $\text{Fe}^{\text{I}}\text{-Fe}^{\text{I}}$ model complexes respectively,^[20] but these are still much higher than the features we see at 1678 and 1711 cm^{-1} . This sug-

Table 1. The photochemistry and assignments of the main observed ^{12}CO bands.

Reactant	MoFe N ₂ ase variant	Reactant bands [cm ⁻¹]	Product bands [cm ⁻¹]	Product bands [cm ⁻¹]	“Free-CO” bands [cm ⁻¹]		
Hi-1	wild-type	1973	1679	Lo-1	1711	2135	2123
	α -H195Q	1969	n.o. ^[a]		1748	2134	2123
Hi-2	wild-type (old)	1938	1874	Lo-2	1784	n.o.	
	α -H195N	1936	1858		1780, 1760	2133	2124
Hi-3	α -H195Q	1932	1864		1748	2134	2123
	α -H195Q	1938	1911	Lo-3	1921	n.o.	

[a] n.o.: not observed.

gests that there is something chemically distinctive about the CO bonding that causes the stretching frequency to move by an extra 100 cm^{-1} , and that invoking lower Fe oxidation states is not enough.

A different type of coordination, with more than two atoms interacting with CO, is one plausible explanation. A doubly bridging CO with either a strong H-bond or an ionic interaction is a possibility. One example is $[\text{Fe}(\text{CO})_3]_2\text{-}[\mu_2\text{-COLi}(\text{THF})_3]_2$, where the Li-coordinated bridging CO molecules have bands reported at 1650 cm^{-1} .^[21] Another possible geometry, with a triply bridging CO perpendicular to a 3-Fe base, is suggested by the known compound $[\text{Fe}(\text{CO})_3]_3(\mu_3\text{-CO})(\mu_3\text{-NSiMe}_3)$.^[22] This complex has a strong CO band at 1743 cm^{-1} as well as a *trans* N that might mimic the unidentified atom “X” in the centre of the FeMo cofactor. The stretching frequency of a triply bridging CO can be driven lower by either side-on or “semi-bridging” metal–CO interactions.^[23] As examples, in $[\text{Cp}_2\text{Rh}_3(\text{CO})_4]^-$, the “semi-triple-bridging” CO has an absorption band at 1693 cm^{-1} ,^[24] whereas in the trinuclear cluster $[\text{PtCo}_2(\text{CO})_5\text{-}(\mu\text{-dppm})_2]$, the band for the “semi-triple-bridging” CO is at 1662 cm^{-1} .^[25] Additional coordination of CO at O, as seen with Li for the semi-triple-bridging CO in $[\{\text{Fe}(\text{CO})_3\}_3\text{-}(\mu_3\text{-COSiMe}_3)\{\mu_3\text{-COLi}(\text{THF})_3\}]$, drives the CO stretching band down to 1647 cm^{-1} .^[26] Thus, from consideration of known chemistry, one viable structure for Hi-1 is that illustrated in part g of Scheme 1. Upon photolysis to Lo-1, the result might resemble that in Scheme 1 (h).

Although such structures are attractive, we must also consider other chemically reasonable possibilities, including metal-formyl complexes (Scheme 1, c). Bound formyl stretching frequencies of $1577\text{--}1607\text{ cm}^{-1}$ were first seen in the kinetically stable formyl complexes, $[\text{Fe}(\text{CO})_4\text{-}(\text{CHO})]^-$.^[27] Later, C=O stretch bands were also assigned in the $1559\text{--}1580\text{ cm}^{-1}$ region for a variety of Fe-formyl complexes.^[28] Finally, C=O stretches associated with $\eta_1\text{-CHO}$ bound to Ru(001) surfaces were seen at 1730 cm^{-1} .^[29] In summary, the range of characteristic formyl frequencies clearly overlaps with the Hi-1 and Lo-1 bands at 1679 and 1711 cm^{-1} .

Hi-2/Lo-2

Our second CO-dependent photolysis signal, Hi-2, is most clearly defined in the $\alpha\text{-H195N}$ “repeat” photolysis difference spectrum (Figure 2). In this spectrum, free of complications from Hi-1 and Hi-3, the primary negative band at 1936 cm^{-1} is associated with a weaker negative band at 1858 cm^{-1} . Similar primary negative bands are observed with $\alpha\text{-H195Q}$ and “aged” wild type N_2ase , at 1932 or 1938 cm^{-1} (Figure 2), each with its own smaller negative feature at 1864 and 1874 cm^{-1} , respectively. These Hi-2 photolysis features are most similar to the bands at 1936 and 1880 cm^{-1} that maximize together over about a minute in SF-FT-IR experiments.^[6]

As for the structures that give rise to these features, for the SF-FT-IR bands at 1936 cm^{-1} and 1880 cm^{-1} , the common time course indicated that these modes arise from a

common species,^[6] and this appears to be a reasonable assumption for the Hi-2 photolysis bands which also appear in common during photolysis (Figure 4). The bands observed in the $1938\text{--}1932\text{ cm}^{-1}$ region are consistent with a terminal assignment for one of the CO molecules in Hi-2. However, the lower frequency ($1858\text{--}1874\text{ cm}^{-1}$) CO bands are significantly shifted from the values most commonly seen for terminal CO. Thus, although a structure with adjacent terminal CO molecules seems plausible, it needs some additional feature to account for the low frequency component of the Hi-2 species.

It is possible that the lower frequency band arises from a bent, semi-bridging geometry. One example of model compound with such CO coordination is $[\text{Fe}_2(\text{S}_2\text{C}_2\text{H}_4)(\text{CO})_3\text{-}(\text{PMe}_3)(\text{dppv})]^+$ which has a CO band at 1883 cm^{-1} . This CO band moves to 1783 cm^{-1} when the CO adopts a fully bridging geometry.^[30] In Av1, a bent geometry leading to semi-bridging interactions could be enforced by a neighbouring ligand. Another alternative is presented by the anionic complex, $[\text{Fe}(\text{NS}_3)(\text{CO})]^-$, where a rare intermediate spin $S = 1$ $\text{Fe}^{\text{II}}\text{-CO}$ species has a CO band at 1885 cm^{-1} in the $[\text{Et}_4\text{N}]^+$ salt.^[31] At this point, there is not enough information to fully define the nature of the low-frequency partner of the Hi-2 pair.

Turning to the photolysis product Lo-2, the band at 1780 cm^{-1} for $\alpha\text{-H195N}$ (1784 or 1748 cm^{-1} in wild-type and $\alpha\text{-H195Q}$ respectively) is consistent with a bridging CO assignment, yielding a structure such as Scheme 1 (b). Conversion of a terminal to a bridging CO was proposed for CO-inhibited Av1 based on ENDOR results, although at that time it was suggested that the bridging CO correlated with the SF-FT-IR band at 1906 cm^{-1} .^[8e] A bridging CO band in the $1748\text{--}1780\text{ cm}^{-1}$ range is easier to defend. In the case of the Hi-2 \rightarrow Lo-2 conversion, one attractive hypothesis is that the distinctive, possibly partially bridging, CO becomes totally bridging when the adjacent terminal CO is photodissociated (Scheme 2). One example of conversion from terminal to bridged CO involves the photolytic and thermal reactions of *trans*- $[\text{Cp}^*\text{Fe}(\text{CO})]_2(\mu\text{-CO})(\mu\text{-CH}_2)$, where loss of one terminal CO from the *trans*-species led to the remaining terminal CO assuming a bridging orientation.^[32]

Hi-3/Lo-3

The cleanest representative of a Hi-3/Lo-3 pair is seen in the $\alpha\text{-H195Q}$ data (Figure 3). Upon first-time photolysis of CO-inhibited $\alpha\text{-H195Q}$ Av1, a negative Hi-3 band at 1938 cm^{-1} is observed, along with a dip at 1911 cm^{-1} and a Lo-3 product peak at 1921 cm^{-1} . On a structural basis, the Hi-3 bands are consistent with a pair of terminal CO molecules, while Lo-3 presumably represents a single terminal CO that remains after photolytic loss of one CO in the pair (Scheme 2).

There are at least two special attributes to this Hi-3 \rightarrow Lo-3 pair. First, Hi-3 \rightarrow Lo-3 conversion is either irreversible, or recombination of the Lo-3 species has a sig-

nificantly higher activation energy than observed with the Lo-2 and Lo-1 species. Such differences are seen in other enzymes, for example, [NiFe] H₂ase.^[33] With this enzyme, photolysis of CO-bound “Ni-SCO” H₂ase yields a dissociated “Ni-SI_a” species, and Ni-SI_a → Ni-SCO recombination has an activation energy of ca. 9 kJ mol⁻¹. In contrast, for Ni-C → Ni-L photolysis, involving dissociation of a “hydrogenic” species, has a higher backreaction activation energy of 46 kJ mol⁻¹. A second special attribute of Hi-3 photolysis is that it leads to a terminal Lo-3 CO product, whereas with Hi-2, the Lo-2 product frequency of ca. 1780 cm⁻¹ suggests a bridging CO product. The special qualities of α -H195Q Av1 that favour Hi-3 and Lo-3 species and their unique properties remain issues to be addressed in future studies.

Connections with Stopped-Flow FT-IR and ENDOR Results

Why is the dominant CO band in the photolysis data of wild-type enzyme at 1973 cm⁻¹, whereas in the SF-FT-IR data, it is near 1936 cm⁻¹? These data suggest that Hi-1 dominates in our frozen samples while Hi-2 is the majority species at room temperature. The same photolysis results were found using rapid freezing in the absence of ethylene glycol, so solvent and timing do not seem to be important factors (Supporting Information). One possibility is simply that freezing changes the relative distribution of the two species. There is ample precedent for changes in the relative population of different species with freezing. As an example, for human wild type MbCO at pH 5.3, form A₀ vs. form A₁ exists as a 27:73 ratio of intensities at 300 K. Upon cooling to 100 K, the relative populations invert so that the A₀ vs. A₁ intensity ratio is now 61:39.^[34] A similar population shift might occur with N₂ase. Needless to say, this increases the complexity of connecting room-temperature measurements, such as reaction kinetics and SF-FT-IR, with the spectroscopy (and crystallography) conducted at low temperatures.

How do the current results connect with EPR/ENDOR spectroscopy, which have been the primary tools for spectroscopic characterization of N₂ase intermediates? EPR spectra of aliquots of the same wild-type CO-inhibited Av1 samples produced for photolysis confirmed that the major paramagnetic species was hi-CO, which was generated in up to about 50–60% yield (Supporting Information). The simplest assumption is that our Hi-1 species, with bands at 1973 and 1679 cm⁻¹, is the same as the hi-CO *S* = 1/2 EPR species. Then, by analogy with EPR-monitored photolytic conversion of hi-CO to lo-CO,^[7] our Lo-1 species with its band at 1711 cm⁻¹ should correlate with the lo-CO EPR species. An attractive feature of this hypothesis is that α -H195N, which does not exhibit the Hi-1 IR signal, also does not exhibit the hi-CO EPR.

Our spectral assignments differ with those made previously,^[8e] where the lo-CO EPR species was correlated with a 1906 cm⁻¹ SF-FT-IR feature, a relatively high frequency for a bridging CO. The hi-CO EPR species was proposed

to contain two terminal CO ligands on separate Fe atoms.^[8e] Our studies indicate that Hi-1 contains two rather different CO species, which might still be consistent with the ENDOR. In our assignment, the hi-CO photolyzable CO at 1973 cm⁻¹ would correspond to CO(2) with ¹³C isotropic hyperfine coupling of 5.4 MHz. Then, our hi-CO non-photolyzable CO at 1679 cm⁻¹ would correspond to CO(1) with ¹³C isotropic hyperfine coupling of 0.7 MHz, and it would remain in the lo-CO form with its ¹³C isotropic hyperfine coupling of 1.2 MHz.^[8e]

If the hi-CO EPR species correlates with our Hi-1 species, then does Hi-2 also relate to a recognized EPR species? The variant α -H195Q Av1 produces the lo-CO and hi(5)-CO EPR signals in addition to the hi-CO signal,^[8g] and it is tempting to associate Hi-2 with the hi(5)-CO EPR species. Although the hi(5)-CO EPR signal is reported not to photolyze,^[8g] this result was obtained with wild-type enzyme, and our clearest examples are with the H195N and H195Q variants. Additional work is needed to clarify this issue.

Our ability to connect Hi-3 with a known EPR signal is even more limited. None of the N₂ase EPR species have been reported to photolyze once and not recombine at 110 K. Despite its unusual behaviour, Hi-3 is a significant fraction of the initial α -H195Q samples. If one assumes equal extinction coefficients for Hi-3 1938 cm⁻¹, Hi-1 1969 cm⁻¹, and Hi-2 1932 cm⁻¹ bands, then Hi-3 is actually the most populated state that we observe in these samples. (This assumption will not hold if some bands represent coupled CO molecules.) Lo-3 is also a mystery; as it is a terminal CO, why does it not also photolyze? The pair are obviously deserving of further study.

CO Pockets and Activation Energies

In all of these cases, where does the photolyzed CO go? The 3–4 kJ mol⁻¹ activation energies for recombination of Lo-1 → Hi-1 and Lo-2 → Hi-2 are similar to the barriers of 2–7 kJ mol⁻¹ for geminate CO recombination in various cytochromes P-450,^[35] and they are less than the ca. 10.5 kJ mol⁻¹ required for recombination from the “docking site” in photolyzed Mb-CO.^[13,36] In Mb, there is a primary docking site above pyrrole C at the periphery of the heme prosthetic group, and a more distant xenon-binding pocket “Xe4” at ca. 9 Å has been implicated in occasional rebinding events.^[13,37] N₂ase also has Xe-binding sites,^[1a] but these are more than 11 Å from the centre of FeMo cofactor. Although they are presumably too far away to be involved in the low activation-energy processes we are seeing, the N₂ase Xe sites might be involved in the residual slower rebinding evident at longer times. A candidate hydrophobic substrate channel has been proposed, terminating near the Fe-2,3,6,7 face and amino acid residues α -V70, α -H195 and α -R96,^[38] as has a more hydrophilic substrate channel, again terminating near the Fe-2,3,6,7 face of the FeMo cofactor.^[39] CO recombination kinetics have been a useful probe of Mb cavities, and in the future, such studies might elucidate similar properties in N₂ase.

Locating CO Binding Sites in the Protein

In this study we have seen that the three N₂ase forms under investigation, wild-type (α -195^{His}), α -H195Q (α -195^{Gln}), and α -H195N (α -195^{Asn}), have rather different CO spectroscopic properties. Before introducing a model to explain these data, we summarize some relevant differences between these proteins. First of all, in the resting state crystal structure, the native enzyme has a key hydrogen bond between its α -195^{His} imidazole side-chain ϵ -N and bridging sulfide S2B of the FeMo cofactor. It has also been proposed that α -195^{His} is involved in proton transfer during substrate reduction.^[15b] Next, as previously noted,^[40] the α -195^{Gln} glutamine side chain of the α -H195Q variant has the same geometric potential for making hydrogen bonds as α -195^{His}, since the chain length to the glutamine amide N is the same as to the imidazole ϵ -N. This prediction was confirmed in the α -H195Q crystal structure, where the glutamine is H-bonded to S2B.^[8g] Despite these similarities, the pK_a for the glutamine primary amide is expected to be > 14, while that for an imidazole ϵ -NH is about 6.2. Finally, the shorter side chain of α -H195N asparagine prevents its amide N from even achieving H-bonding proximity. Thus, our 3 different proteins have 3 very different H donor capabilities. It is also known that α -H195Q has very poor N₂ reduction activity compared to wild-type, while α -H195N can bind N₂ but cannot reduce it at all.^[40]

The α -195 residues are located near the Fe-2,3,6,7 face that has been implicated in substrate binding.^[1c] In a recent stopped-flow IR study, we showed that substitutions at α -70^{Val}, which lies approximately above Fe-6, have dramatic effects on the CO IR spectra.^[6d] In particular, substitution by a bulkier α -70^{Ile} results in slower generation of the 1936 cm⁻¹ band, indicating steric hindrance for creation of this CO species.

Apart from the site-directed mutagenesis studies, extensive computational work has been done by Dance using “*in silico* cofactor transplantation”, in which DFT structures of ligated FeMo cofactor are embedded into the protein binding site.^[41] The η^1 (end-on) N₂ binding studied by Dance should have similar dimensions to the terminal CO bonds observed by IR. Three acceptable modes of end-on binding were discovered – “*exo*” (approximately *trans* to interstitial X) at Fe2 or Fe6, and “*endo*” (approximately *trans* to a bridging S) at Fe 2. The “*exo*” binding geometry at Fe2 was excluded because of unacceptable interference with α -195^{His}. Ligands in the “*endo*” positions at either Fe2 or Fe6 were observed to be directed towards the α -70^{Val} side-chain.

From all of the above, it is possible to make a working model for plausible geometries of CO binding (Figure 5). Whereas the schematic structures in Scheme 2 are intentionally vague and limited so as to capture what is unambiguous from the spectroscopy, the proposed structure in Figure 5 is admittedly speculative, but it takes into account the known data and can be used to formulate new experiments. We use the IR results that indicate the presence of terminal and/or bridging CO in various species. Following our recent stopped-flow IR results,^[6d] we place these ligands on the

Fe-2,3,6,7 face proposed by Seefeldt and co-workers as the key site for substrate interactions. The terminal CO is placed on Fe6, since this site is the least hindered and has a pocket that could accommodate a free CO upon photolysis. It is also the site favored by Dance for terminal N₂ binding. A CO-bound in the “*exo*” geometry at Fe6 is also in good position to hydrogen bond with the amide side chain of α -191^{Gln} or with a homocitrate carboxylate. In fact, substitution by lysine in the α -Q191K variant produces a protein incapable of binding more than one CO or producing the hi-CO or hi(5)-CO EPR signals.^[8h] Finally, we place the bridging CO between Fe2 and Fe6. Although this was originally done to allow for H bonding with α -195^{His}, another more likely possibility to be considered is H bonding with α -359^{Arg}.

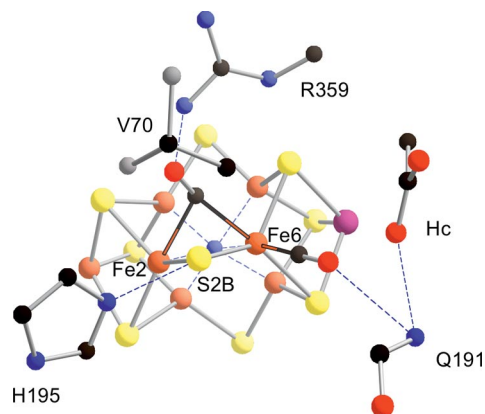


Figure 5. One (of many) candidate structures for CO-inhibited N₂ase. No attempt has been made to optimize FeMo cofactor or protein atom positions, both of which likely change upon CO binding. Atom color codings: Fe orange, Mo purple, S yellow, C black, O red. The undefined central atom of FeMo-co is shown in blue.

Implications for N₂ Chemistry

Even though CO is not reduced by Mo N₂ases, the existence of a species with a substantially lowered CO stretching frequency may well have relevance for the N₂ase mechanism. It may also be directly relevant to the recent report of CO reduction to ethylene, ethane, and propane with V N₂ase.^[3] The observed Hi-1 and Lo-1 intermediates may also be relevant to Fischer–Tropsch chemistry, where metal-formyls have also been frequently invoked as catalytic intermediates.^[42] In this context, it may be that multi- or semi-bridging CO and formyl-bound formulations are not mutually exclusive – it is plausible that a multi- or semi-bridging interaction between two or more metals on the FeMo cofactor is what allows creation of a formyl complex. However, it may well be that N₂ase has insufficient driving force to complete the thermodynamically uphill reduction of CO to HCHO (H₂ + CO = HCHO, $\Delta G^\circ_{(227^\circ\text{C})} = +51$ kJ/mol).^[43] So, a bound formyl on Mo N₂ase might be expected to decompose back to CO and hydride with ultimate H₂ evolution, whereas with N₂ an analogous bound HN₂ species might be produced on the way to the final NH₃ product.

Conclusions

FT-IR spectroscopic monitoring of the photolysis of CO-inhibited Mo-N₂ase has revealed three distinct types of CO complexes for this enzyme under hi-CO conditions. We have labelled these stable inhibited forms Hi-1, Hi-2, and Hi-3. Each of these species has at least two bands, indicating at least two types of CO, and each has a photolyzed product, Lo-1, Lo-2, and Lo-3 with a band indicating at least one remaining CO.

Hi-1 is best seen in wild-type Av1, and it has a conventional terminal CO band at 1973 cm⁻¹, as well as a unique feature at 1679 cm⁻¹, perhaps indicative of a protonated doubly bridging CO, a triply-bridging CO, or even a formyl species. Hi-2 is most clearly seen with α -H195N Av1, and it has bands at 1932 and 1858 cm⁻¹. Hi-3 is a very different species, best seen on the first photolysis of α -H195Q Av1, and it has bands at 1936 and 1911 cm⁻¹. The respective photoproducts, Lo-1, Lo-2, and Lo-3, occur at very different values at 1711, 1780, and 1921 cm⁻¹. Along with bound CO molecules, two bands near 2123 and 2135 cm⁻¹ have been seen after photolysis. These most likely representing forms of “free-CO” in different orientations, akin to the forms of photolyzed CO in myoglobin pockets.

Another surprise was that in the wild-type enzyme, Hi-2 appears to dominate the room temperature SF-FT-IR results while the frozen solutions studied here only contain Hi-1. This apparent temperature dependence has clear implications for the comparison of room temperature techniques with the many spectroscopies, and even protein crystallography, which use frozen samples and cryogenic temperatures.

In general, we have discovered that FT-IR-monitored photolysis of CO-bound to Mo-N₂ase is an information-rich approach. Overall, 11 significantly different types of CO bands have so far been observed with many additional minor species not counted – an unexpected plethora of CO interactions with this enzyme. Additional studies are planned both to reconcile the results with those from other spectroscopic techniques and to probe other important aspects of nitrogenase catalysis.

Experimental Section

General: *Azotobacter vinelandii* Mo N₂ase, as well as the α -H195N and α -H195Q variants were prepared as described in the Supporting Information. In each case, the hi-CO complex was prepared from a turnover mixture in the presence of 100% CO under low electron flux conditions obtained with a 1:4 molar ratio of Fe:MoFe proteins. The reaction was quenched by the addition of ethylene glycol to a final concentration of 40%, and the product was concentrated in an Amicon microfiltration pressure concentrator under 100% of the appropriate CO isotope.

Samples for FTIR analysis were placed in custom cell holders with Teflon spacers and either zinc sulfide (Del Mar Photonics) or cubic zirconia windows. Typical pathlengths ranged from 50–15 μ m. FTIR spectra were measured in a Bruker VERTEX 70v FT-IR spectrometer equipped with a custom adapted Oxford Instruments CF1208 liquid-helium flow cryostat. Photolysis with visible light

employed an Osram XENOPHOT® lamp (100 W) or a Sutter Instruments Lambda LS xenon arc lamp (300 W).

Supporting Information (see footnote on the first page of this article): Full experimental details.

Acknowledgments

This work was funded by the National Institutes of Health (NIH) (grant number GM-65440, to S. P. C.), the National Science Foundation (NSF) (grant number CHE-0745353, to S. P. C.), and by the DOE Office of Biological and Environmental Research (to S. P. C.).

- [1] a) D. C. Rees, F. A. Tezcan, C. A. Haynes, M. Y. Walton, S. Andrade, O. Einsle, J. B. Howard, *Phil. Trans. R. Soc. A* **2005**, *363*, 971–984; b) J. W. Peters, R. K. Szilagy, *Curr. Opin. Chem. Biol.* **2006**, *10*, 101–108; c) B. M. Barney, H.-I. Lee, P. C. D. Santos, B. M. Hoffman, D. R. Dean, L. C. Seefeldt, *Dalton Trans.* **2006**, 2277–2284; d) I. Dance, *Chem. Asian J.* **2007**, *2*, 936–946; e) L. C. Seefeldt, B. M. Hoffman, D. R. Dean, *Ann. Rev. Biochem.* **2009**, *78*, 701–722.
- [2] a) B. M. Barney, D. Lukoyanov, T. C. Yang, D. R. Dean, B. M. Hoffman, L. C. Seefeldt, *Proc. Natl. Acad. Sci. USA* **2006**, *103*, 17113–17118; b) D. Lukoyanov, B. M. Barney, D. R. Dean, L. C. Seefeldt, B. M. Hoffman, *Proc. Natl. Acad. Sci. USA* **2007**, *104*, 1451–1455; c) B. M. Barney, J. McCleod, D. Lukoyanov, M. Laryukhin, T.-C. Yang, D. R. Dean, B. M. Hoffman, L. C. Seefeldt, *Biochemistry* **2007**, *46*, 6784–6794.
- [3] C. C. Lee, Y. Hu, M. W. Ribbe, *Science* **2010**, *329*, 642.
- [4] C. J. Lind, P. W. Wilson, *J. Am. Chem. Soc.* **1941**, *63*, 3511–3514.
- [5] J. C. Hwang, C. H. Chen, R. H. Burris, *Biochim. Biophys. Acta* **1973**, *292*, 256–270.
- [6] a) S. J. George, G. A. Ashby, C. W. Wharton, R. N. F. Thorneley, *J. Am. Chem. Soc.* **1997**, *119*, 6450–6451; b) R. N. F. Thorneley, S. J. George, in: *Time Resolved Infra-red Spectroscopy of Functioning Nitrogenase* (Ed.: E. W. Triplett), Horizon Scientific Press, Wymondham, UK, **2000**, pp. 81–99; c) J. D. Tolland, R. N. F. Thorneley, *Biochemistry* **2005**, *44*, 9520–9527; d) Z.-Y. Yang, L. C. Seefeldt, D. R. Dean, S. P. Cramer, S. J. George, *Angew. Chem. Int. Ed.* **2011**, *50*, 272–275.
- [7] Z. Maskos, B. J. Hales, *J. Inorg. Biochem.* **2003**, *93*, 11–17.
- [8] a) L. C. Davis, M. T. Henzl, R. H. Burris, W. H. Orme-Johnson, *Biochemistry* **1979**, *18*, 4860–4869; b) V. G. Moore, R. C. Tittsworth, B. J. Hales, *J. Am. Chem. Soc.* **1994**, *116*, 12101–12102; c) R. C. Pollock, H. I. Lee, L. M. Cameron, V. J. Deroose, B. J. Hales, W. H. Orme-Johnson, B. M. Hoffman, *J. Am. Chem. Soc.* **1995**, *117*, 8686–8687; d) P. D. Christie, H. I. Lee, L. M. Cameron, B. J. Hales, W. H. Orme-Johnson, B. M. Hoffman, *J. Am. Chem. Soc.* **1996**, *118*, 8707–8709; e) H.-I. Lee, L. M. Cameron, B. J. Hales, B. M. Hoffman, *J. Am. Chem. Soc.* **1997**, *119*, 10121–10126; f) L. M. Cameron, B. J. Hales, *Biochemistry* **1998**, *37*, 9449–9456; g) M. Sørli, J. Christiansen, B. J. Lemon, J. W. Peters, D. R. Dean, B. J. Hales, *Biochemistry* **2001**, *40*, 1540–1549; h) Z. Maskos, K. Fisher, M. Sørli, W. E. Newton, B. J. Hales, *J. Biol. Inorg. Chem.* **2005**, *10*, 394–406.
- [9] C. J. Pickett, K. A. Vincent, S. K. Ibrahim, C. A. Gormal, B. E. Smith, S. P. Best, *Chem. Eur. J.* **2003**, *9*, 76–87.
- [10] M. C. Durrant, *Biochemistry* **2004**, *43*, 6030–6042.
- [11] T. H. Rod, J. K. Nørskov, *J. Am. Chem. Soc.* **2000**, *122*, 12751–12763.
- [12] M. L. McKee, *J. Comput. Chem.* **2007**, *28*, 1342–1356.
- [13] K. Nienhaus, G. U. Nienhaus, in: *Ligand dynamics in heme proteins observed by Fourier transform infrared spectroscopy at cryogenic temperatures*, vol. 437, Elsevier Academic Press Inc., San Diego, **2008**, pp. 347–378.
- [14] a) K. A. Bagley, C. J. Vangarderen, M. Chen, E. C. Duin, S. P. J. Albracht, W. H. Woodruff, *Biochemistry* **1994**, *33*, 9229–

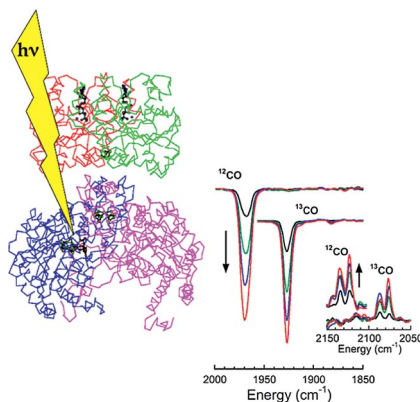
- 9236; b) Z. J. Chen, B. J. Lemon, S. Huang, D. J. Swartz, J. W. Peters, K. A. Bagley, *Biochemistry* **2002**, *41*, 2036–2043.
- [15] a) C.-H. Kim, W. E. Newton, D. R. Dean, *Biochemistry* **1995**, *34*, 2798–2808; b) K. Fisher, M. J. Dilworth, C. Kim, W. E. Newton, *Biochemistry* **2000**, *39*, 2970–2979.
- [16] a) A. Barth, *Prog. Biophys. Mol. Biol.* **2000**, *74*, 141–173; b) A. Barth, *Biochim. Biophys. Acta* **2007**, *1767*, 1073–1101.
- [17] M. C. Durrant, *Biochem. J.* **2001**, *355*, 569–576.
- [18] a) T. S. Li, M. L. Quillin, G. N. Phillips, J. S. Olson, *Biochemistry* **1994**, *33*, 1433–1446; b) J. D. Müller, B. H. McMahon, E. Y. T. Chien, S. G. Sligar, G. U. Nienhaus, *Biophys. J.* **1999**, *77*, 1036–1051.
- [19] a) W. Roseboom, A. L. De Lacey, V. M. Fernandez, E. C. Hat-chikian, S. P. J. Albracht, *J. Biol. Inorg. Chem.* **2006**, *11*, 102–118; b) A. Silakov, C. Kamp, E. Reijerse, T. Happe, W. Lubitz, *Biochemistry* **2009**, *48*, 7780–7786.
- [20] M. Razavet, S. J. Borg, S. J. George, S. P. Best, S. A. Fairhurst, C. J. Pickett, *Chem. Commun.* **2002**, 700–701.
- [21] B. Neumüller, W. Petz, *Organometallics* **2001**, *20*, 163–170.
- [22] E. von Gustorf, R. Wagner, *Angew. Chem. Int. Ed. Engl.* **1971**, *10*, 910.
- [23] a) F. A. Cotton, *Prog. Inorg. Chem.* **1976**, *21*, 1–28; b) R. H. Crabtree, M. Lavin, *Inorg. Chem.* **1986**, *25*, 805–812.
- [24] W. D. Jones, M. A. White, R. G. Bergman, *J. Am. Chem. Soc.* **1978**, *100*, 6770–6772.
- [25] P. Braunstein, C. D. Debellefon, B. Oswald, *Inorg. Chem.* **1993**, *32*, 1649–1655.
- [26] W. Petz, B. Neumuller, *Z. Anorg. Allg. Chem.* **2007**, *633*, 2032–2036.
- [27] J. P. Collman, S. R. Winter, *J. Am. Chem. Soc.* **1973**, *95*, 4089–4090.
- [28] C. P. Casey, M. W. Meszaros, S. M. Neumann, I. G. Cesa, K. J. Haller, *Organometallics* **1985**, *4*, 143–149.
- [29] W. J. Mitchell, Y. Wang, J. Xie, W. H. Weinberg, *J. Am. Chem. Soc.* **1993**, *115*, 4381–4382.
- [30] A. K. Justice, T. B. Rauchfuss, S. R. Wilson, *Angew. Chem.* **2007**, *119*, 6264; *Angew. Chem. Int. Ed.* **2007**, *46*, 6152–6154.
- [31] S. C. Davies, M. C. Durrant, D. L. Hughes, R. L. Richards, J. R. Sanders, *J. Chem. Soc., Dalton Trans.* **2000**, 4694–4701.
- [32] Y. H. Spooner, E. M. Mitchell, B. E. Bursten, *Organometallics* **1995**, *14*, 5251–5257.
- [33] M.-E. Pandelia, H. Ogata, W. Lubitz, *ChemPhysChem* **2010**, *11*, 1127–1140.
- [34] S. Balasubramanian, D. G. Lambright, S. G. Boxer, *Proc. Natl. Acad. Sci. USA* **1993**, *90*, 4718–4722.
- [35] C. Tétreau, C. DiPrimo, R. Lange, H. Tourbez, D. Lavalette, *Biochemistry* **1997**, *36*, 10262–10275.
- [36] P. J. Steinbach, K. Chu, H. Frauenfelder, J. B. Johnson, D. C. Lamb, G. U. Nienhaus, T. B. Sauke, R. D. Young, *Biophys. J.* **1992**, *61*, 235–245.
- [37] a) R. F. Tilton, I. D. Kuntz, G. A. Petsko, *Biochemistry* **1984**, *23*, 2849–2857; b) K. Nienhaus, P. C. Deng, J. M. Kriegl, G. U. Nienhaus, *Biochemistry* **2003**, *42*, 9647–9658; c) D. R. Nutt, M. Meuwly, *Biophys. J.* **2003**, *85*, 3612–3623; d) M. Meuwly, *Eur. Phys. J. Special Top.* **2007**, *141*, 209–216.
- [38] R. Y. Igarashi, L. C. Seefeldt, *Crit. Rev. Biochem. Mol. Biol.* **2003**, *38*, 351–384.
- [39] B. M. Barney, M. G. Yurth, P. C. Dos Santos, D. R. Dean, L. C. Seefeldt, *J. Biol. Inorg. Chem.* **2009**, *14*, 1015–1022.
- [40] K. Fisher, M. J. Dilworth, W. E. Newton, *Biochemistry* **2000**, *39*, 15570–15577.
- [41] I. Dance, *J. Am. Chem. Soc.* **2007**, *129*, 1076–1088.
- [42] a) C. Masters, in: *The Fischer–Tropsch Reaction*, vol. 17 (Eds.: F. G. A. Stone, W. Robert), Academic Press, **1979**, pp. 61–103; b) E. L. Muettterties, J. Stein, *Chem. Rev.* **1979**, *79*, 479–490; c) E. de Smit, B. M. Weckhuysen, *Chem. Soc. Rev.* **2008**, *37*, 2758–2781.
- [43] P. M. Maitlis, *J. Mol. Catal. A* **2003**, *204–205*, 55–62.

Received: January 10, 2011

Published Online: ■

Nitrogenase Chemistry

Fourier transform infrared spectroscopy (FT-IR) has been used to study the photochemistry at cryogenic temperatures of CO-inhibited *Azotobacter vinelandii* nitrogenase MoFe protein as well as α -H195Q and α -H195N variant proteins. The observed spectra allow the identification of 11 distinct CO-bound species. The spectra can be interpreted in terms of a combination of terminal, multiply bridged and possibly protonated CO species bound to the FeMo cofactor active site.



L. Yan, C. H. Dapper, S. J. George,
H. Wang, D. Mitra, W. Dong,
W. E. Newton, S. P. Cramer* 1–12

Photolysis of Hi-CO Nitrogenase – Observation of a Plethora of Distinct CO Species Using Infrared Spectroscopy

Keywords: Nitrogen fixation / Nitrogenases / Enzyme catalysis / Carbon monoxide / IR spectroscopy / Photolysis / *Azotobacter vinelandii*